Published OnlineFirst July 14, 2010; DOI: 10.1158/0008-5472.CAN-10-0999

Therapeutics, Targets, and Chemical Biology

Cancer Research

Vorinostat and Sorafenib Increase CD95 Activation in Gastrointestinal Tumor Cells through a Ca^{2+}-*De novo* Ceramide-PP2A-Reactive Oxygen Species–Dependent Signaling Pathway

Margaret A. Park[1], Clint Mitchell[1], Guo Zhang[1], Adly Yacoub[1], Jeremy Allegood[1], Dieter Häussinger[6], Roland Reinehr[6], Andrew Larner[1], Sarah Spiegel[1], Paul B. Fisher[3,4], Christina Voelkel-Johnson[5], Besim Ogretmen[5], Steven Grant[1,2,3], and Paul Dent[1,3]

Abstract

The targeted therapeutics sorafenib and vorinostat interact in a synergistic fashion to kill carcinoma cells by activating CD95, and this drug combination is entering phase I evaluation. In this study, we determined how CD95 is activated by treatment with this drug combination. Low doses of sorafenib and vorinostat, but not the individual drugs, rapidly increased reactive oxygen species (ROS), Ca^{2+}, and ceramide levels in gastrointestinal tumor cells. The production of ROS was reduced in Rho zero cells. Quenching ROS blocked drug-induced CD95 surface localization and apoptosis. ROS generation, CD95 activation, and cell killing was also blocked by quenching of induced Ca^{2+} levels or by inhibition of PP2A. Inhibition of acidic sphingomyelinase or *de novo* ceramide generation blocked the induction of ROS; however, combined inhibition of both acidic sphingomyelinase and *de novo* ceramide generation was required to block the induction of Ca^{2+}. Quenching of ROS did not affect drug-induced ceramide/dihydro-ceramide levels, whereas quenching of Ca^{2+} reduced the ceramide increase. Sorafenib and vorinostat treatment radiosensitized liver and pancreatic cancer cells, an effect that was suppressed by quenching ROS or knockdown of LASS6. Further, sorafenib and vorinostat treatment suppressed the growth of pancreatic tumors *in vivo*. Our findings show that induction of cytosolic Ca^{2+} by sorafenib and vorinostat is a primary event that elevates dihydroceramide levels, each essential steps in ROS generation that promotes CD95 activation. *Cancer Res; 70(15); 6313–24. ©2010 AACR.*

Introduction

In the United States, hepatoma and pancreatic carcinomas have 5-year survival rates of <10% and <5%, respectively (1, 2). These statistics emphasize the need to develop novel therapies against these lethal malignancies.

The extracellular signal-regulated kinase 1/2 (ERK1/2) pathway is frequently dysregulated in neoplastic transformation (3–5). The ERK1/2 module comprises, along with c-Jun NH_2-terminal kinase (JNK1/2) and p38 mitogen-activated protein kinase (MAPK), members of the MAPK super family. These kinases are involved in responses to diverse mitogens and stresses, and have also been implicated in survival processes. Activation of the ERK1/2 pathway is generally associated with survival, whereas induction of JNK1/2 and p38 MAPK pathways generally signals apoptosis. Although the mechanisms by which ERK1/2 activation promote survival are not fully characterized, several antiapoptotic effector proteins have been identified, including increased expression of antiapoptotic proteins such as c-FLIP (6–11).

Sorafenib is a multikinase inhibitor that was originally developed as an inhibitor of Raf-1, but which was subsequently shown to inhibit multiple other kinases, including class III tyrosine kinase receptors such as platelet-derived growth factor (PDGF), vascular endothelial growth factor (VEGF) receptors 1 and 2, c-Kit, and FLT3 (12–14). The antitumor effects of sorafenib in renal cell carcinoma and in hepatoma have been ascribed to antiangiogenic actions of this agent through inhibition of the growth factor receptors (15–17). Several groups have shown *in vitro* that sorafenib kills human leukemia cells at concentrations below the maximum achievable dose (C_{max}) of 15 to 20 μmol/L, through a mechanism involving the downregulation of the antiapoptotic BCL-2 family member MCL-1 (18, 19). In these studies sorafenib-mediated MCL-1 downregulation occurred through a translational rather than a transcriptional or

Authors' Affiliations: Departments of [1]Biochemistry, [2]Medicine, [3]VCU Institute of Molecular Medicine, and [4]Human and Molecular Genetics, Virginia Commonwealth University, Richmond, Virginia; [5]Medical University of South Carolina, Charleston, South Carolina; and [6]Clinic for Gastroenterology, Hepatology and Infectiology, Heinrich-Heine-University Dusseldorf, Dusseldorf, Germany

Note: Supplementary data for this article are available at Cancer Research Online (http://cancerres.aacrjournals.org/).

Corresponding Author: Paul Dent, Department of Biochemistry and Molecular Biology, 401 College Street, Massey Cancer Center, Room 280a, Box 980035, Virginia Commonwealth University, Richmond, VA 23298-0035. Phone: 804-628-0861; Fax: 804-827-1309; E-mail: pdent@vcu.edu.

doi: 10.1158/0008-5472.CAN-10-0999

Published OnlineFirst July 14, 2010; DOI: 10.1158/0008-5472.CAN-10-0999

posttranslational process that was mediated by endoplasmic reticulum (ER) stress signaling (20, 21). This suggests that the previously observed antitumor effects of sorafenib are mediated by a combination of inhibition of *Raf* family kinases, receptor tyrosine kinases that signal angiogenesis, and the induction of ER stress signaling.

Histone deacetylase inhibitors (HDACI) represent a class of agents that act by blocking histone deacetylation, thereby modifying chromatin structure and gene transcription. HDACIs promote histone acetylation and neutralization of positively charged lysine residues on histone tails, allowing chromatin to assume a more open conformation, which favors transcription (22). HDACIs also induce acetylation of other nonhistone targets, actions that may have plieotropic biological consequences, including inhibition of HSP90 function, induction of oxidative injury, and upregulation of death receptor expression (23–25). With respect to combinatorial drug studies with a multikinase inhibitor such as sorafenib, HDACIs are of interest in that they also downregulate multiple oncogenic kinases by interfering with HSP90 function, leading to proteasomal degradation of these proteins. Vorinostat (Zolinza) is a hydroxamic acid HDACI that has shown preliminary preclinical evidence of activity in hepatoma and other malignancies with a C_{max} of ~9 μmol/L (26–28).

We have recently published that sorafenib and vorinostat interact to kill in a wide range of tumor cell types through activation of the CD95 extrinsic apoptotic pathway (29, 30). The present studies have extended in greater molecular detail our analyses to understanding how sorafenib and vorinostat interact to promote CD95 activation.

Materials and Methods

Materials

Sorafenib tosylate (Bayer) and vorinostat (Merck) were provided by the Cancer Treatment and Evaluation Program, National Cancer Institute/NIH. Commercially available validated short hairpin RNA molecules to knock down RNA/protein levels were from Qiagen: CD95 (SI02654463; SI03118255). The kit to assay PP2A activity was purchased from Millipore. Reagents and performance of experimental procedures were described in refs. 20, 21, 29–37.

Cell line authentication

HEPG2, HEP3B, Mia PaCa2, and PANC1 cells were purchased from the American Type Culture Collection on a regular basis (fresh cryo-preserved vials of cells have been purchased at least once every 6 mo). Cells have not been authenticated in the corresponding author's laboratory.

Culture and *in vitro* exposure of cells to drugs

Cells were cultured as described refs. 29–32.

In vitro cell treatments

Cells were isolated at the indicated times and subjected to trypan blue cell viability assay by counting in a light microscope, or alternatively, Annexin V/propidium iodide assays were carried to confirm our cell viability data (29–32).

Transfection of cells with small interfering RNA or with plasmids

Transfections were performed as described in refs. 29–32.

Assessment of reactive oxygen species generation and cytosolic Ca^{2+} levels

Cancer cells were plated in 96-well plates. Cells were preincubated with dihydro-DCF (5 mmol/L for 30 min). Fluorescence measurements were obtained 0 to 30 minutes after drug addition with a Vector 3 plate reader. Data are presented corrected for basal fluorescence of vehicle-treated cells at each time point and expressed as a fold increase in reactive oxygen species (ROS) levels. Carcinoma cells, seeded in 96-well plates, with fura-2 acetoxymethylester as an indicator. The ratio of Fura-2 acetoxymethylester emissions, when excited at the wavelengths of 340 and 380 nm, was recorded, and analysis software were used to process and statistically analyze data.

Mass spectrometric analysis of sphingolipids and metabolites

Cells were washed extensively with PBS and detached by trypsinization. An aliquot of cells was taken for protein determination. For the remainder of cells, internal standards were added; lipids were extracted; and individual ceramide acyl chain species were quantified by liquid chromatography, electrospray ionization tandem mass spectrometry (29).

Recombinant adenoviral vectors; infection *in vitro*

Cells were infected with adenoviruses at an approximate multiplicity of infection of 50 (29–32).

Animal studies

Mia Paca2 cells were injected s.c. (1×10^7), and 14 days later, tumor volume was determined by calipers. Animals were segregated into four groups of approximate mean tumor volume ± SEM and then treated by oral gavage with vehicle or sorafenib+vorinostat. Animals are treated once per day for 5 consecutive days. Twenty-four hours after the first drug administration, animals are placed in a shielded container and either mock exposed or have the flanks irradiated (2 Gy). Forty-eight hours after the first irradiation, a second irradiation (2 Gy) is performed. Tumors were subjected to two cycles of drug treatment/radiation exposure (total dose 4 × 2 Gy). Tumor mass is determined at least every 3rd day after the initiation of drug treatment.

Data analysis

Comparison of the effects of various treatments was performed using ANOVA and the Student's *t* test. Differences with a P value of <0.05 were considered statistically significant. All experiments were performed on at least two separate occasions: each cell death or ceramide measurement experiment had between 3 and 4 separate independent experimental data points per experiment, and each ROS or Ca^{2+} measurement had at least 8 to 12 independent data points per experiment. Thus, experiments shown are the means of multiple individual data points per experiment from multiple experiments (±SEM).

Published OnlineFirst July 14, 2010; DOI: 10.1158/0008-5472.CAN-10-0999

Results

Treatment of cells with low concentrations of sorafenib and vorinostat, but not the individual agents, promoted activation of CD95 and the generation of ROS (Fig. 1A and B). The rapid activation of CD95 was not reduced by incubation with a neutralizing antibody to inhibit FAS ligand (data not shown). The production of ROS was quenched using N-acetyl cysteine or MnTBAP (Fig. 1C). Mitochondria-deficient rho zero HuH7 cells were generated (29–32); cells lacking functional mitochondria exhibited a significantly reduced ability to generate ROS in response to sorafenib and vorinostat exposure (Fig. 1D).

Quenching of drug-induced ROS suppressed sorafenib and vorinostat toxicity (Fig. 2A and B). Quenching of ROS also suppressed CD95 activation (Fig. 2B, inset). Molecular quenching of ROS using thioredoxin (TRX) suppressed ROS generation, CD95 activation, and drug toxicity, whereas molecular enhancement of ROS generation through expression of a mutant-inactive TRX protein enhanced ROS generation, although not CD95 activation, and promoted drug toxicity (Fig. 2C). HuH7 hepatoma cells do not express CD95 and are relatively resistant to sorafenib and vorinostat-induced cell killing (29). Transfection of HuH7 cells with a wild-type CD95-YFP construct, but not a construct lacking two known sites of regulatory tyrosine phosphorylation CD95-YFP FF, facilitated sorafenib and vorinostat toxicity (Fig. 2D). Sorafenib and vorinostat treatment promoted tyrosine phosphorylation and cell surface localization of wild-type CD95-YFP but not of CD95-YFP YY-FF (data not shown; Fig. 2D).

Low concentrations of either sorafenib (1–3 μmol/L) or vorinostat (250–500 nmol/L) did not strongly increase either ROS or Ca^{2+} levels, whereas we did observe, at 9 to 12 μmol/L sorafenib and >1 μmol/L vorinostat concentrations, measurable effects of the individual drugs on ROS and Ca^{2+} levels (data not shown). Treatment of tumor cells with low doses of sorafenib and vorinostat enhanced cytosolic Ca^{2+} levels (Fig. 3A). Quenching of ROS did not block drug-induced cytosolic Ca^{2+} levels (Fig. 3B). Quenching of Ca^{2+}, using either BAPTA-AM or expression of Calbindin D28, blocked drug-induced ROS induction (data not shown; Fig. 3C). Expression of Calbindin D28 blocked endogenous CD95 surface localization, CD95 tyrosine phosphorylation, and CD95 association with caspase-8 (Fig. 3D, top section). Expression of Calbindin D28 blocked sorafenib and vorinostat toxicity (Fig. 3D, bottom graph). Knockdown of CD95 neither blocked drug-induced cytosolic Ca^{2+} levels nor blocked capacitative Ca^{2+} entry into cells (Supplementary Figs. S1–S3).

Prior studies using sorafenib and vorinostat had implicated ceramide as a mediator of CD95 activation. Loss of acidic sphingomyelinase expression (ASMase −/−) caused a partial although statistically significant ($P < 0.05$) reduction in drug-induced cytosolic Ca^{2+} levels (Fig. 4A). In contrast to the partial effect observed on reducing Ca^{2+} levels, deletion of ASMase expression abolished drug-induced ROS production (Fig. 4B). Knockdown of ASMase or inhibition of the *de novo* ceramide synthase pathway each caused a partial reduction in drug-induced cytosolic Ca^{2+} levels, and complete blockade of ceramide generation abolished Ca^{2+} induction (Fig. 4C). Combined knockdown of ASMase expression and inhibition of *de novo* ceramide synthesis in hepatoma cells abolished sorafenib- and vorinostat-induced ROS levels (Fig. 4D).

We next wished to place the sequence of ceramide generation within the context of elevated ROS and Ca^{2+} levels. Knockdown of CD95 protected tumor cells from sorafenib+vorinostat toxicity (Fig. 5A). CD95 activation and sorafenib+vorinostat toxicity were blocked by knockdown of ASMase and by inhibition of *de novo* ceramide synthesis (Fig. 5B). Knockdown of ceramide synthase 6 (LASS6) expression abolished drug-induced activation of CD95 and significantly reduced drug toxicity (Fig. 5C). Inhibition of ROS generation did not alter sorafenib+vorinostat-induced C16 ceramide or dihydro-ceramide levels (Fig. 5D). However, inhibition of drug-induced cytosolic Ca^{2+} levels or knock down of LASS6 significantly reduced the amount of C16 dihydro-ceramide generated following drug treatment (data not shown; Fig. 5D). In parallel studies using SW620 colon cancer cells that lack LASS6 expression, transfected to express LASS6, we noted that re-expression of ceramide synthase 6 restored drug-induced ROS generation levels (Supplementary Fig. S4).

As sorafenib+vorinostat exposure generated ceramide, and the protein serine/threonine phosphatase PP2A can play a pivotal role in ceramide-dependent signaling, as well as in the regulation of ROS generation, we determined whether modulation of PP2A function affected the actions of this drug combination (29, 37). Sorafenib and vorinostat activated PP2A in a LASS6-dependent fashion (Fig. 6A). Expression of a wild-type PP2A inhibitory protein, whose function can be blocked by ceramide or a mutant inhibitor protein, whose function cannot be altered by ceramide, suppressed drug combination–induced ROS generation and cell death (Fig. 6B and C). Phosphorylation of mitochondria-localized signal transducers and activators of transcription 3 (STAT3) S727 plays a key role in regulating the rate of mitochondrial respiration and *de facto* mitochondrial ROS production, and STAT3 S727 is a PP2A substrate (38). Sorafenib and vorinostat treatment reduced STAT3 S727 phosphorylation by ~50% within 2 hours (Fig. 6D). Expression of a dominant-negative form of STAT3 S727A enhanced sorafenib and vorinostat lethality, whereas expression of activated STAT3 S727D suppressed drug toxicity (Fig. 6D).

Sorafenib and HDACI drug combination therapy is entering clinical phase I evaluation. Radiotherapy is known to generate ROS and ceramide, and it is a primary therapeutic modality for pancreatic cancer. Sorafenib and vorinostat treatment radiosensitized pancreatic and liver cancer cells *in vitro* (Supplementary Figs. S5 and S6). Radiosensitization was blocked by expression of TRX or knockdown of LASS6 expression (Supplementary Fig. S5). Treatment of animals carrying MiaPaca2 tumors with sorafenib and vorinostat significantly reduced tumor growth *in vivo*, which validates this

Published OnlineFirst July 14, 2010; DOI: 10.1158/0008-5472.CAN-10-0999

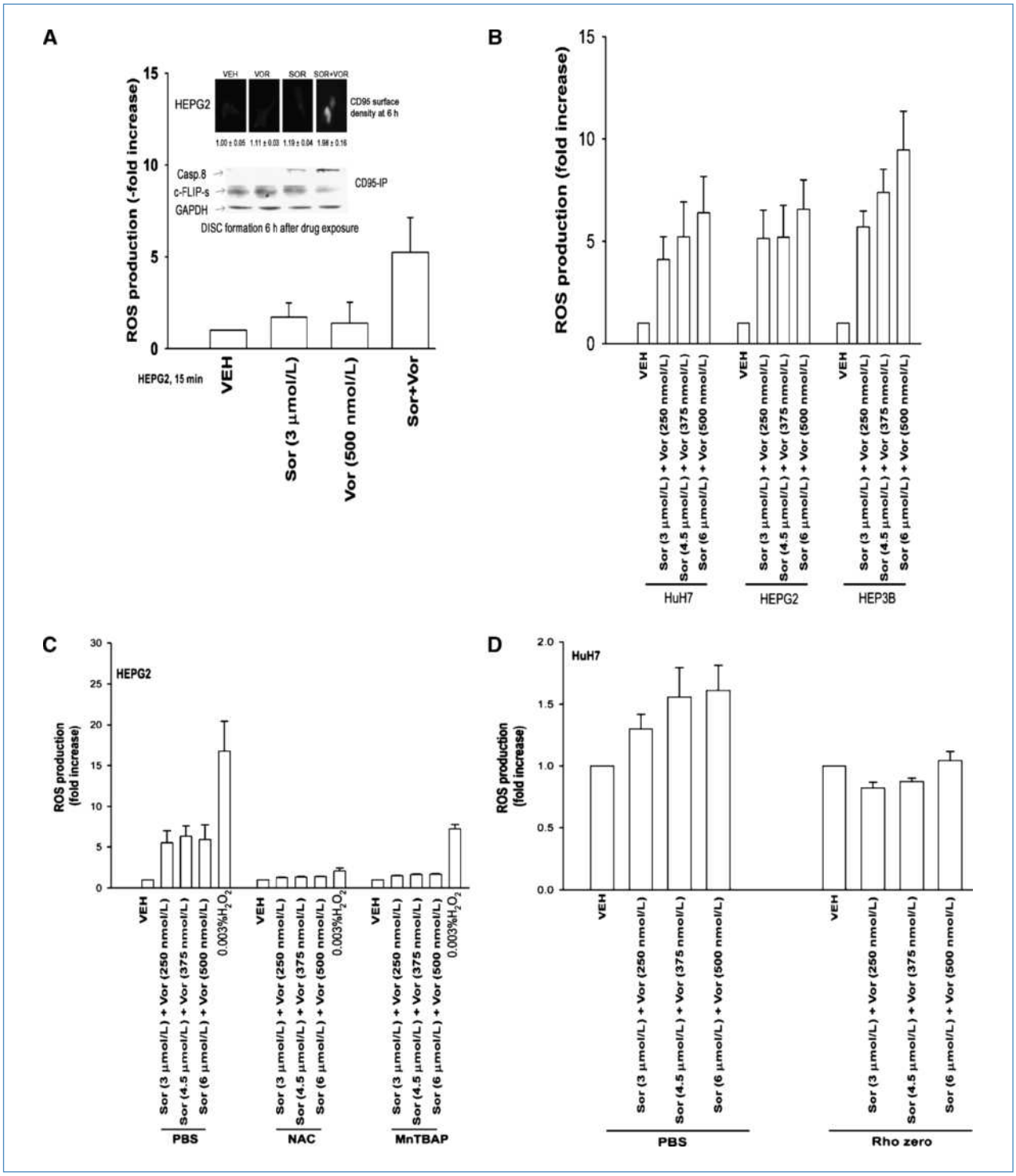

Figure 1. Sorafenib and vorinostat interact to increase ROS levels in GI tumor cells. A, HEPG2 cells were treated with vehicle (DMSO), sorafenib (Sor), vorinostat (Vor), or in combination. ROS levels were measured 15 min after exposure and plotted as the fold increase (n = 2, ±SEM). Top, HEPG2 cells were treated with sorafenib, vorinostat, or the combination, and, 6 h after, exposure cells were fixed and CD95 surface levels determined by immunohistochemistry (IHC); HEPG2 cells were treated with vehicle (DMSO), sorafenib, vorinostat,or the combination, and, 6 h after, exposure cells were lysed and CD95 were immunoprecipitated followed by immunoblotting of the precipitate for DISC formation. B, cells were treated with vehicle (DMSO), sorafenib, and vorinostat. ROS levels were measured 15 min after exposure and plotted as the fold increase (n = 2, ±SEM). C, HEPG2 cells were treated with vehicle (PBS), N-acetyl cysteine, or MnTBAP followed 30 min later by sorafenib and vorinostat. ROS levels were measured 15 min after exposure and plotted as the fold increase (n = 2, ±SEM). D, HuH7 parental and rho zero hepatoma cells were treated with vehicle (DMSO), sorafenib, and vorinostat. ROS levels were measured 15 min after exposure and plotted as the fold increase (n = 2, ± SEM).

Published OnlineFirst July 14, 2010; DOI: 10.1158/0008-5472.CAN-10-0999

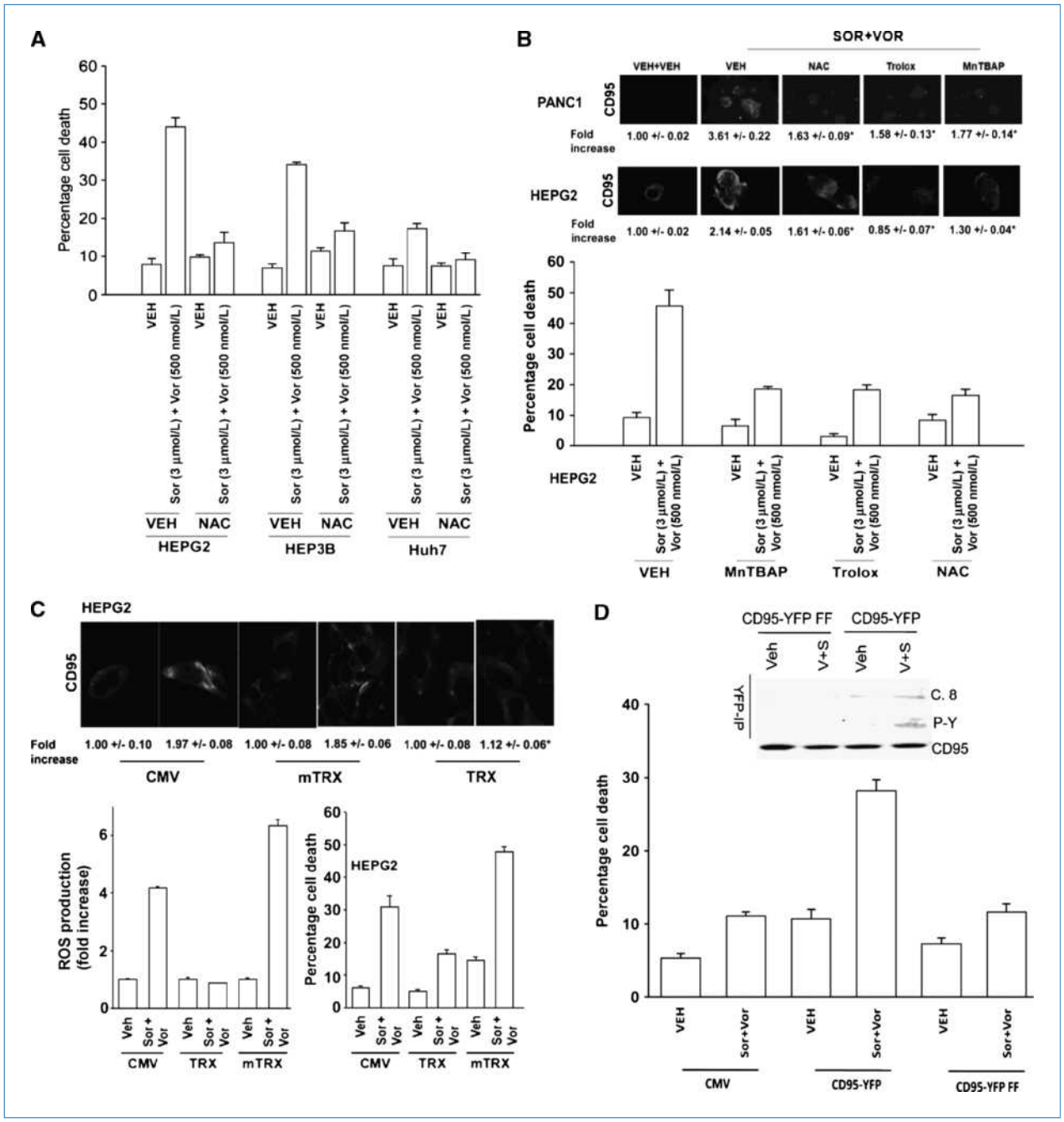

Figure 2. ROS play a central role in CD95 activation and apoptosis. A, hepatoma cells were pretreated with N-acetyl cysteine and then with sorafenib and vorinostat. Viability was determined by trypan blue after 48 h (n = 3, ± SEM). B, bottom, HEPG2 cells were pretreated with N-acetyl cysteine, Trolox, or MnTBAP, and with sorafenib and vorinostat. ROS levels were measured 15 min after exposure (n = 2, ± SEM). Top IHC, PANC1 and HEPG2 cells were pretreated with N-acetyl cysteine, Trolox, or MnTBAP and, 30 min later, treated with sorafenib and vorinostat. Cells were fixed after 6 h, and cell surface CD95 levels were determined. C, bottom graphs, left, HEPG2 cells were transfected with empty vector (CMV) or to express either wild-type TRX or mutant inactive TRX (mTRX). Twenty-four hours after transfection, cells were treated with sorafenib (3.0 μmol/L) and vorinostat (500 nmol/L). ROS levels were measured 15 min after treatment (n = 2, ±SEM); right, HEPG2 cells were transfected to express either TRX or mTRX. Twenty-four hours after transfection, cells were treated with sorafenib, vorinostat, or both drugs. Cells were isolated after 48 h, and viability was determined by trypan blue (n = 3, ± SEM). Top IHC, HEPG2 cells were transfected to express TRX or mTRX. Twenty-four hours after transfection, cells were treated with sorafenib and vorinostat. Six hours after treatment, cells were fixed and CD95 plasma membrane levels were determined (n = 2, ± SEM). D, bottom graph, HuH7 cells were transfected to express CD95-YFP or CD95-YFP FF. Twenty-four hours after transfection, cells were treated with sorafenib (3.0 μmol/L) and vorinostat (500 nmol/L). Cells were isolated after 48 h, and viability was determined by trypan blue (n = 2, ± SEM). Top, HuH7 cells were transfected to express CD95-YFP or CD95-YFP FF. Twenty-four hours after transfection, cells were treated with sorafenib and vorinostat. Cells were isolated after 6 h and CD95 immunoprecipitated to determine DISC formation and CD95 tyrosine phosphorylation.

Published OnlineFirst July 14, 2010; DOI: 10.1158/0008-5472.CAN-10-0999

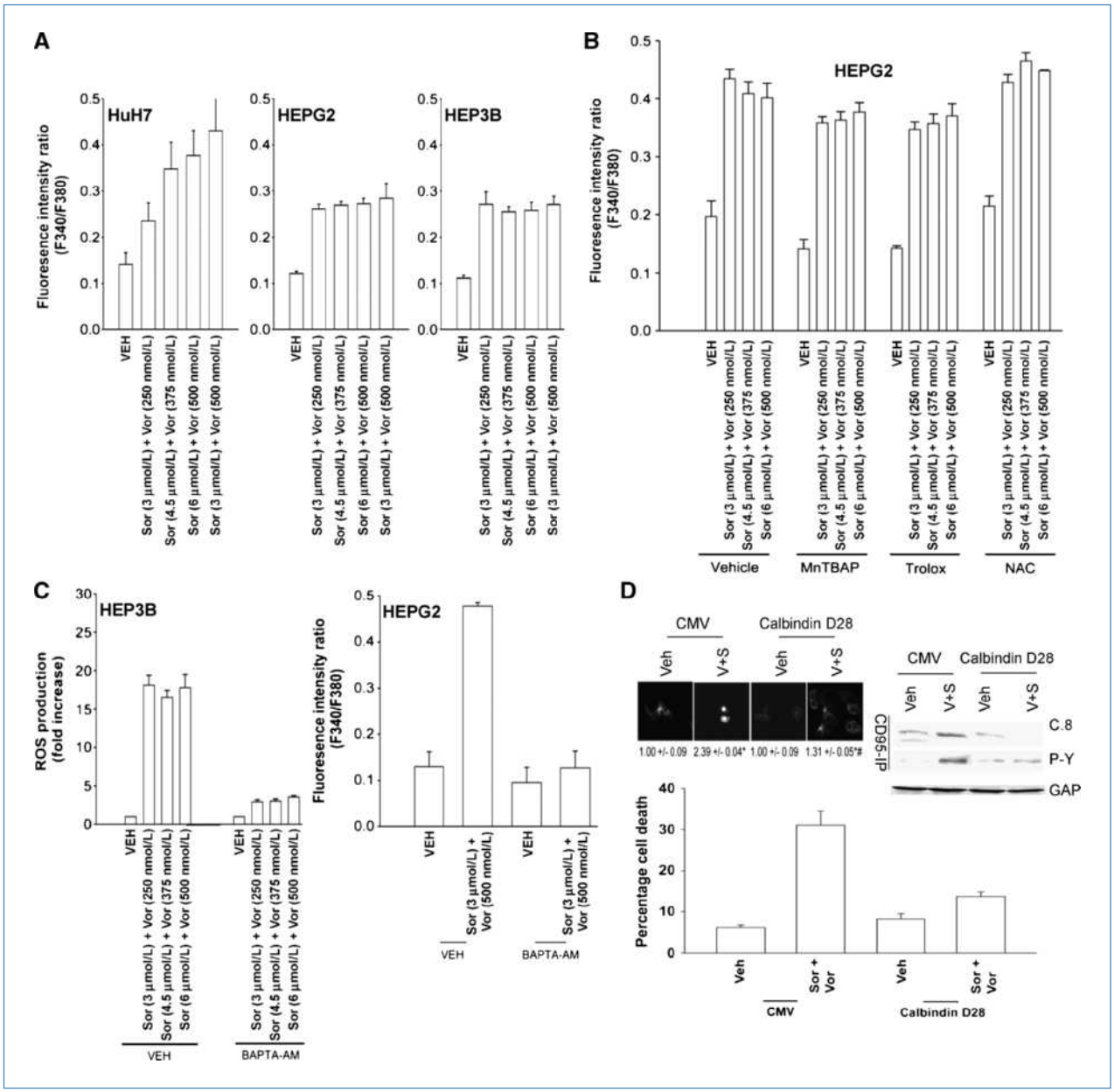

Figure 3. Sorafenib and vorinostat treatment modulates Ca^{2+} signaling. A, hepatoma cells were treated with sorafenib and vorinostat. Cytosolic Ca^{2+} levels were measured 15 min after exposure and plotted as the fluorescence intensity ratio (n = 2, ± SEM). B, HEPG2 cells were pretreated with MnTBAP, N-acetyl cysteine, or Trolox followed 30 min later by treatment with sorafenib and vorinostat. Cytosolic Ca^{2+} levels were measured 15 min after exposure (n = 2, ± SEM). C, left, HEP3B cells were preincubated in Ca^{2+}-free media for 1 h before addition of BAPTA-AM or vehicle. Ten minutes after, BAPTA-AM additions were treated with sorafenib and vorinostat or with $CaCl_2$. ROS levels were measured 15 min after exposure (n = 2, ± SEM). Right, HEPG2 cells were preincubated in Ca^{2+}-free media for 1 h before addition of BAPTA-AM or vehicle. Ten minutes after, BAPTA-AM additions were treated with sorafenib and vorinostat. Cytosolic Ca^{2+} levels were measured 15 min after exposure (n = 2, ± SEM). D, top CD95 IHC, HEPG2 cells were transfected to express Calbindin D28 and, 24 h later, were treated with sorafenib (3 μmol/L) and vorinostat (500 nmol/L). Six hours after exposure, cells were fixed, and the levels of plasma membrane CD95 were determined (n = 2, ± SEM). Blotting, HEPG2 cells were transfected to express Calbindin D28 and, 24 h later, were treated with sorafenib and vorinostat. Six hours after exposure, cells were isolated, CD95 were immunoprecipitated, and DISC were formation determined (n = 3). Bottom, HEPG2 cells were transfected to express Calbindin D28 and, 24 h later, were treated with sorafenib and vorinostat. Cells were isolated 48 h later, and viability was determined by trypan blue (n = 2, ± SEM).

drug combination as a possible therapeutic for pancreatic cancer ($P < 0.05$; Supplementary Fig. S7). Tumor growth was blunted by radiation exposure; however, radiation exposure did not significantly further enhance the antitumor effects of sorafenib and vorinostat treatment on tumor regrowth. Further studies will be required to determine whether the *in vivo* administration of radiotherapy combined with drug treatment is schedule dependent.

Published OnlineFirst July 14, 2010; DOI: 10.1158/0008-5472.CAN-10-0999

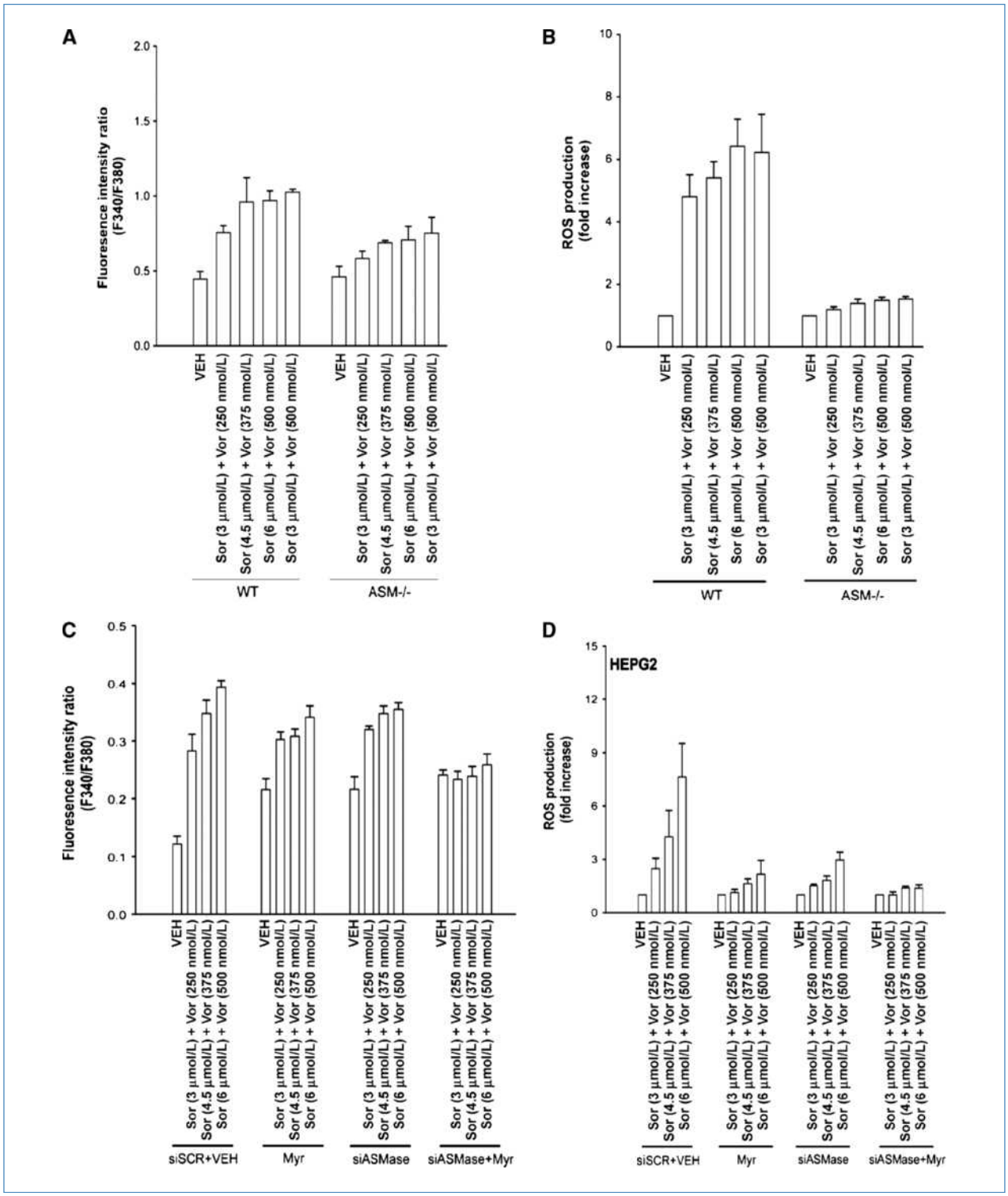

Figure 4. ROS generation is ceramide dependent. A, primary mouse hepatocytes (wild-type and acidic sphingomyelinase–null) were treated with sorafenib and vorinostat. Cytosolic Ca^{2+} levels were measured 15 min after exposure (n = 2, ± SEM). B, primary mouse hepatocytes were treated with sorafenib and vorinostat. ROS levels were measured 15 min after drug exposure (n = 2, ± SEM). C, HEPG2 cells were transfected with a small interfering RNA to knock down ASMase. Twenty-four hours later, cells were treated with myriocin and were then treated with sorafenib and vorinostat. Cytosolic Ca^{2+} levels were measured 15 min after drug exposure (n = 2, ± SEM). D, HEPG2 cells were transfected with a small interfering RNA to knock down ASMase. Twenty-four hours later, cells were treated with myriocin as indicated and were then treated with sorafenib and vorinostat. ROS levels were measured 15 min after drug exposure (n = 2, ± SEM).

Published OnlineFirst July 14, 2010; DOI: 10.1158/0008-5472.CAN-10-0999

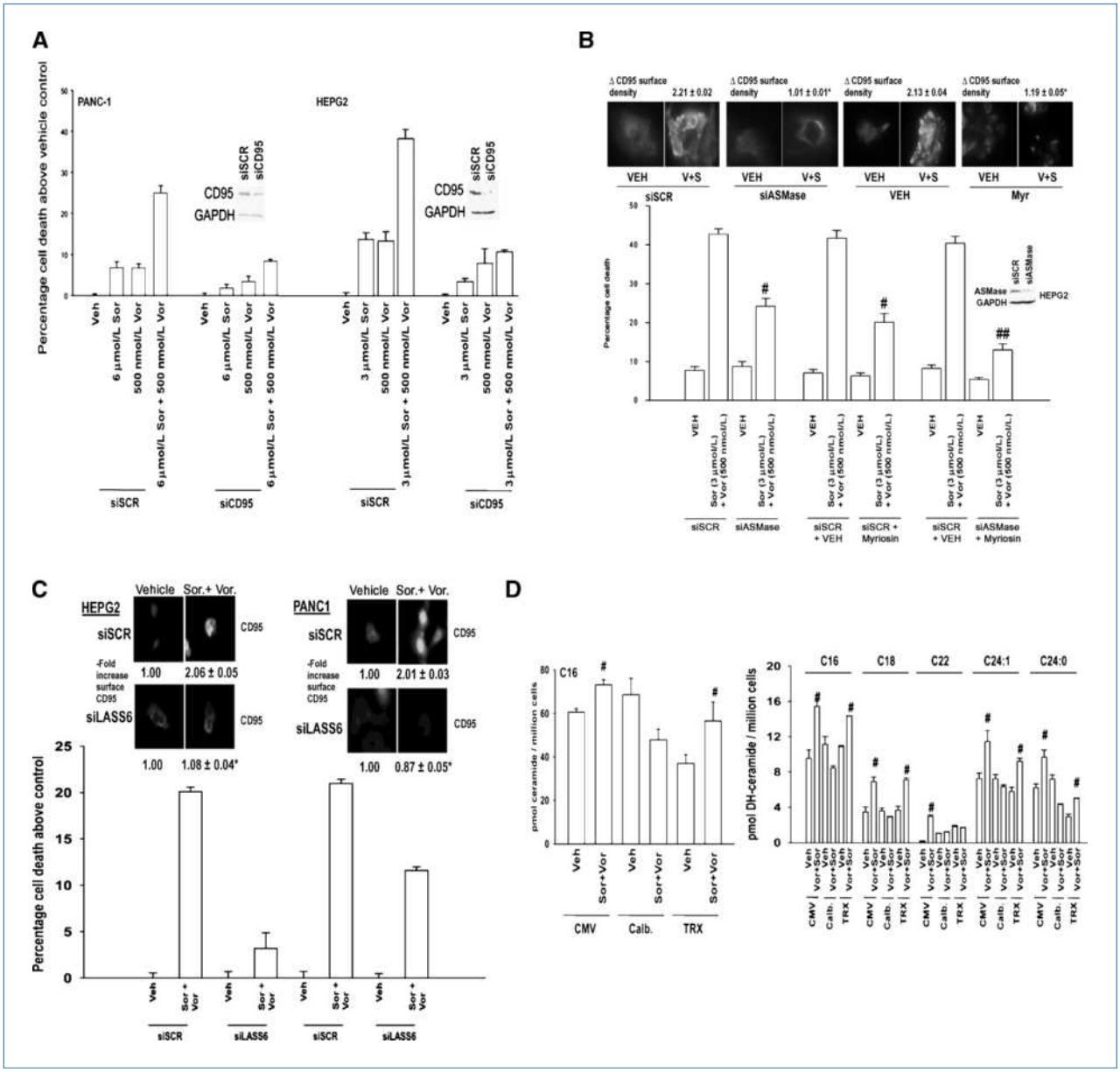

Figure 5. Codependent ceramide and Ca^{2+} regulation of CD95 activity and GI tumor cell killing. A, HEPG2 and PANC-1 cells were transfected to knock down the expression of CD95. Cells were treated 24 h after transfection with sorafenib, vorinostat, or both drugs. Viability was determined by trypan blue after 48 h (n = 3, ± SEM). B, HEPG2 cells were transfected to knock down the expression ASMase. Cells were treated 24 h after transfection with myriocin and 30 min later with sorafenib and vorinostat. Top IHC, cells were transfected as indicated and, 24 h later, treated with drugs. After 6 h, cells were fixed and CD95 plasma membrane levels were determined (n = 3, ± SEM). Bottom, 48 h after exposure, viability was determined by trypan blue (n = 3, ± SEM). C, HEPG2 and PANC-1 cells were transfected to knock down the expression of LASS6. Cells were treated 24 h after transfection with sorafenib and vorinostat. Top IHC, 6 h after exposure, cells were fixed and the levels of plasma membrane were CD95 determined (n = 3, ± SEM). Bottom, 48 h after drug exposure, viability was determined by trypan blue (n = 3, ± SEM). D, HEPG2 cells were transfected with plasmids to express Calbindin D28 or TRX. Twenty-four hours after transfection, cells were treated with sorafenib and vorinostat. Six hours after treatment, cells were taken and lysed and processed to isolate the lipid fraction of the cell. The levels of C16 ceramide and C16-C24:0 dihydroceramide were determined using a tandem mass spectrometer as described in Materials and Methods (n = 2, ± SEM). #, $P < 0.05$ greater than corresponding vehicle-treated value.

Discussion

The present studies attempted to determine in detail the molecular mechanisms by which sorafenib and vorinostat interacted to activate CD95 and promote drug-induced toxicity. Low concentrations of sorafenib and vorinostat interacted in a greater than additive manner to increase ROS levels. The induction of ROS occurred in cells lacking expression of CD95, strongly arguing against death receptor–induced activation of NADPH oxidases in this process. In rho zero cells, the

Published OnlineFirst July 14, 2010; DOI: 10.1158/0008-5472.CAN-10-0999

induction of ROS was reduced, arguing that mitochondria represent the major source of drug-induced ROS generation. Quenching of ROS blocked CD95 activation and drug combination–induced cell death. Sorafenib and vorinostat treatment increased cytosolic Ca^{2+} levels in an ROS-independent fashion, and quenching of Ca^{2+} blocked the increase in ROS levels, CD95 activation, and tumor cell killing. Inhibition of ASMase or of *de novo* ceramide generation almost abolished drug combination–induced ROS levels and CD95 activation, but individually blockade of either pathway only caused a partial suppression in drug-induced cytosolic Ca^{2+}. Quenching of Ca^{2+}, or knockdown of ceramide synthase 6, reduced drug-induced ceramide levels. Thus, our data argue for drug combination–induced Ca^{2+} signaling (primary) and

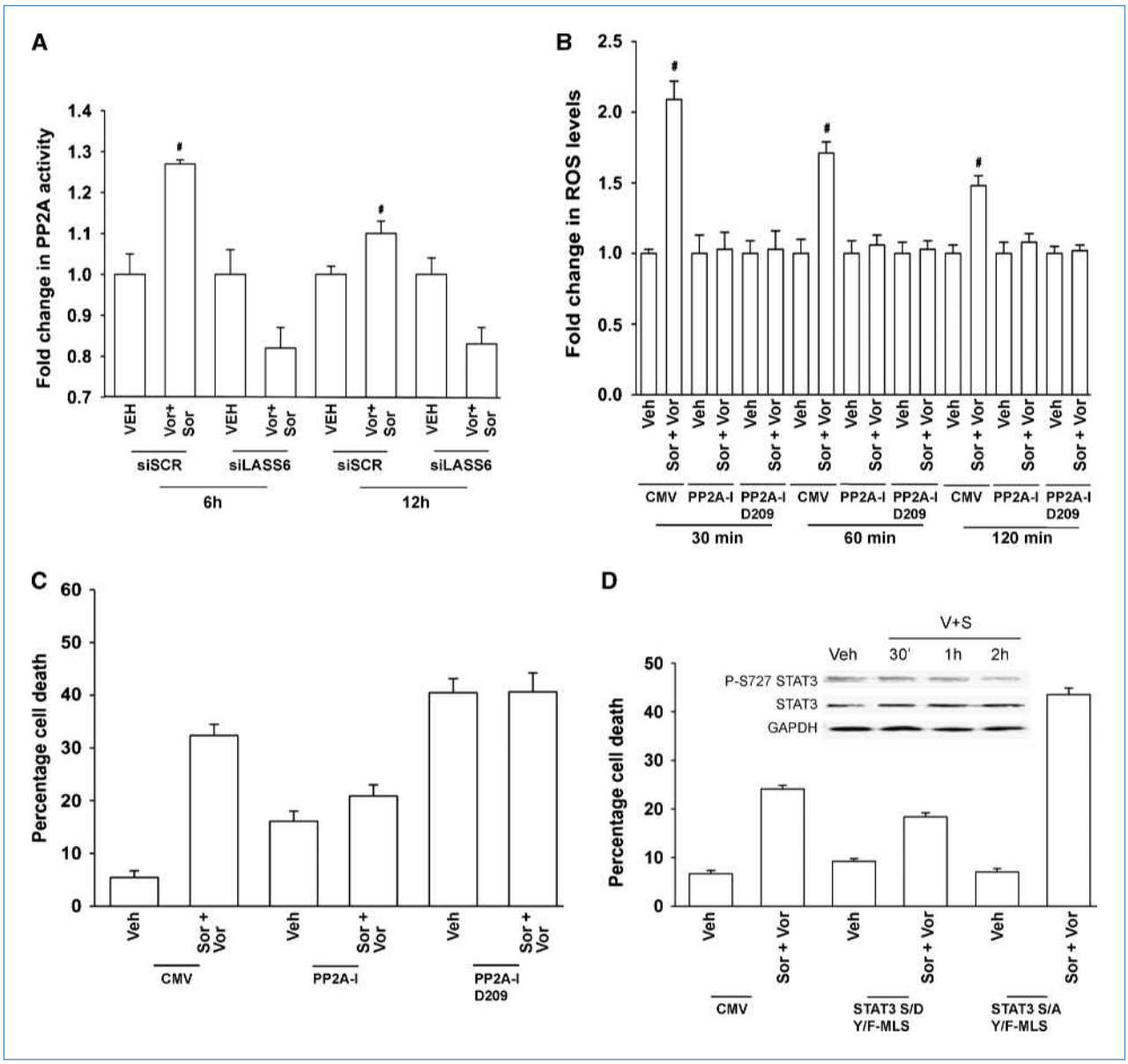

Figure 6. Sorafenib and vorinostat treatment activates PP2A in a LASS6-dependent fashion: PP2A activation is essential for enhanced ROS levels. A, HEPG2 cells were transfected to knock down LASS6 expression (siLASS6). Twenty-four hours after transfection, cells were treated with sorafenib and vorinostat. Cells were processed for PP2A activity according to the manufacturer's instructions. Data are the fold change in PP2A activity ($n = 2$, ± SEM); #, $P < 0.05$ greater than corresponding vehicle-treated value. B, HEPG2 cells were transfected with plasmids to express wild-type or mutant D209 PP2A inhibitor proteins. ROS levels were measured 15 min after drug exposure ($n = 2$, ± SEM). C, HEPG2 cells were transfected with plasmids to express wild-type or mutant D209 PP2A inhibitor proteins. Twenty-four hours after transfection, cells were treated with sorafenib and vorinostat. Cells were isolated and viability determined by trypan blue after 48 h ($n = 3$, ± SEM). D, HEPG2 cells were transfected with plasmids to express mitochondria-localized STAT3 S727A or STAT3 S727D. Twenty-four hours after transfection, cells were treated with sorafenib and vorinostat. Viability was determined by trypan blue after 48 h ($n = 3$, ± SEM). Top, inset, HEPG2 cells were treated with sorafenib and vorinostat, and cells were isolated at the indicated times and the levels of STAT3 S727, total STAT3, and glyceraldehyde-3-phosphate dehydrogenase (GAPDH; $n = 3$).

Published OnlineFirst July 14, 2010; DOI: 10.1158/0008-5472.CAN-10-0999

ceramide generation (secondary) as two interdependent signaling processes that regulate each other, and that both signals act in concert to promote ROS generation, which is essential for drug-induced CD95 activation and tumor cell death (Supplementary Fig. S8).

Bile acids can promote ligand-independent, ASMase, and ceramide-dependent activation of CD95 in hepatocytes (11, 34–39). The generation of ceramide has been shown by many groups to promote ligand-independent activation of growth factor receptors through the clustering of these receptors and other signal facilitating proteins into lipid rich domains (39). The six known ceramide synthase genes (*LASS*) are localized in the ER, and different LASS proteins have been noted to generate different chain length ceramide forms (40). Based on our data, with increases in C16 dihydro-ceramide levels, it was probable that vorinostat and sorafenib were modulating the activities of LASS6 and LASS5, respectively (40). We identified ceramide synthase 6 (LASS6) as an essential enzyme in the drug-induced induction of ceramide, in CD95 activity, and in tumor cell killing. Treatment of cells with vorinostat increased the acetylation of LASS6, suggesting that one mechanism of drug-induced LASS6 activity may be mediated in part through this process.[7] It is well known that other nonhistone proteins are functionally regulated by reversible acetylation, notably NFκB and HSP90 (22–25). Additional studies will be required to define the precise site of acetylation in LASS6 and to discover whether it truly is a site of regulatory acetylation.

The generation of ROS was significantly reduced in rho zero cells, and we have documented a key role for mitochondria in the production of ROS in response to various agents (e.g., ref. 41). In the present studies, ROS production was a tertiary effect dependent on the actions of ceramide and Ca^{2+}. It has been widely documented that the release of Ca^{2+} from the ER in to the cytosol rapidly alters Ca^{2+} levels in mitochondria, and that changes in Ca^{2+} fluxes within mitochondria can stimulate ROS production (e.g., ref. 42). Ceramide levels, independently of Ca^{2+} fluxes, are causal in regulating mitochondrial ROS production, and we noted that whereas inhibition of both ASMase and *de novo* ceramide generation was required to suppress Ca^{2+} signaling, inhibition of either *de novo* or ASMase actions blocked ROS production. There are several probable modes of ceramide action at the mitochondrion that could alter respiratory chain complex activities, including modulation of membrane fluidity as well as activation of PP2A (37, 43–45). The mitochondrial respiratory chain complexes, as well as BCL-2 family proteins, are heavily Ser/Thr phosphorylated, and ceramide has the potential to regulate their function through PP2A. In this regard, drug treatment reduced STAT3 S727 phosphorylation, and inhibition of PP2A activity blocked sorafenib+vorinostat-induced ROS and suppressed drug toxicity. The additional molecular targets of PP2A beyond STAT3 in the regulation of mitochondrial ROS generation will be explored in future studies.

Ligand-independent activation of CD95 is a complex process, including tyrosine phosphorylation, altered subcellular localization and formation of the DISC, i.e., association with FADD and procaspase-8 (37, 38). In our system, drug-induced activation of CD95, as defined by formation of the DISC or by plasma membrane localization of CD95, was blocked by quenching of Ca^{2+}, suppressing ceramide formation or by quenching ROS production. Tyrosine phosphorylation of CD95 was essential for drug-induced membrane localization and DISC formation, but tyrosine phosphorylation of CD95 was only suppressed by quenching Ca^{2+}. Thus, at least two independent signals downstream of drug-induced Ca^{2+} signaling act to promote ligand-independent activation of CD95 in GI tumor cells. The regulation of CD95 tyrosine phosphorylation has been proposed to be catalyzed by ERBB1 and by Src family tyrosine kinases (38).

An additional question that remains unresolved is how sorafenib and vorinostat treatment promote Ca^{2+} signaling, and what the putative primary effectors for these drugs are. Two likely targets of sorafenib and vorinostat may be LASS6 and the IP_3 receptors that regulate ER Ca^{2+} fluxes. At present, little is known about how the ceramide synthase proteins are enzymatically regulated, and it is possible that sorafenib reduces phosphorylation at a regulatory site or, alternatively, that vorinostat promotes LASS6 acetylation, which facilitates enzyme activation. Whether Ca^{2+}-calmodulin signaling directly or through CaM kinase actions modulates ceramide synthase function is unknown. It is also possible that the drug combination causes inactivation of ceramidase enzyme activities that act to lower ceramide levels. IP_3 levels are regulated by phospholipase C and phosphodiesterase enzymes; at present, the effect of sorafenib and vorinostat exposure on the activities of peritoneal lymphocytes (PLC) enzymes is unclear, and data from many groups arguing that sorafenib inhibits receptor tyrosine kinases such as the PDGF and VEGF receptors, and c-Kit would *a priori* predict for reduced activity of PLC enzymes that would reduce IP_3 levels (14, 15).

Sorafenib and HDACI combination therapy is entering phase I evaluation at both Virginia Commonwealth University and at Medical University of South Carolina in a variety of solid and liquid tumor types. We have noted that sorafenib and vorinostat combination therapy shows *in vitro* efficacy against multiple pancreatic cancer cell lines (29, 30, 46). The present studies showed that sorafenib and vorinostat treatment suppressed the growth of pancreatic tumor cells *in vivo*, potentially validating this drug combination as a new therapeutic for pancreatic cancer. Further studies, however, will be required to determine whether sorafenib and HDACI combination therapy can radiosensitize GI tumors in a sequence-dependent fashion *in vivo*.

Disclosure of Potential Conflicts of Interest

No potential conflicts of interest were disclosed.

Grant Support

This work was funded by PHS grants R01-DK52825, P01-CA104177, and R01-CA108520 (P. Dent).

The costs of publication of this article were defrayed in part by the payment of page charges. This article must therefore be hereby marked *advertisement* in accordance with 18 U.S.C. Section 1734 solely to indicate this fact.

Received 03/23/2010; revised 05/24/2010; accepted 06/03/2010; published OnlineFirst 07/14/2010.

[7] Unpublished observations.

Published OnlineFirst July 14, 2010; DOI: 10.1158/0008-5472.CAN-10-0999

References

1. Parkin DM, Bray F, Ferlay J, Pisani P. Global cancer statistics, 2002. CA Cancer J Clin 2005;55:74–108.
2. Bilimoria KY, Bentrem DJ, Lillemoe KD, Talamonti MS, Ko CY, Pancreatic Cancer Quality Indicator Development Expert Panel, American College of Surgeons. Assessment of pancreatic cancer care in the United States based on formally developed quality indicators. J Natl Cancer Inst 2009;101: 848–59.
3. Dent P. MAP kinase pathways in the control of hepatocyte growth, metabolism and survival. In: Dufour JF, Clavien P-A, editors. Signaling Pathways in Liver Diseases. New York: Springer Press; 2005. Chapter 19, p. 223–38.
4. Dent P, Yacoub A, Fisher PB, Hagan MP, Grant S. MAPK pathways in radiation responsesOncogene 2003;22:5885–96.
5. Valerie K, Yacoub A, Hagan MP, et al. Radiation-induced cell signaling: inside-out and outside-in. Mol Cancer Ther 2007;6: 789–801.
6. Grant S, Dent P. Kinase inhibitors and cytotoxic drug resistance. Clin Cancer Res 2004;10:2205–7.
7. Allan LA, Morrice N, Brady S, Magee G, Pathak S, Clarke PR. Inhibition of caspase-9 through phosphorylation at Thr 125 by ERK MAPK. Nat Cell Biol 2003;5:647–54.
8. Mori M, Uchida M, Watanabe T, et al. Activation of extracellular signal-regulated kinases ERK1 and ERK2 induces Bcl-xL up-regulation via inhibition of caspase activities in erythropoietin signaling. J Cell Physiol 2003;195:290–7.
9. Ley R, Balmanno K, Hadfield K, Weston C, Cook SJ. Activation of the ERK1/2 signaling pathway promotes phosphorylation and proteasome-dependent degradation of the BH3-only protein, Bim. J Biol Chem 2003;278:18811–6.
10. Wang YF, Jiang CC, Kiejda KA, Gillespie S, Zhang XD, Hersey P. Apoptosis induction in human melanoma cells by inhibition of MEK is caspase-independent and mediated by the Bcl-2 family members PUMA, Bim, and Mcl-1. Clin Cancer Res 2007;13: 4934–42.
11. Qiao L, Han SI, Fang Y, et al. Bile acid regulation of C/EBPβ CREB, c-Jun function, via the extracellular signal-regulated kinase and c-Jun NH2-terminal kinase pathways, modulates the apoptotic response of hepatocytes. Mol Cell Biol 2003;23: 3052–66.
12. Li N, Batt D, Warmuth M. B-Raf kinase inhibitors for cancer treatment. Curr Opin Investig Drugs 2007;8:452–6.
13. Davies BR, Logie A, McKay JS, et al. AZD6244 (ARRY-142886), a potent inhibitor of mitogen-activated protein kinase/extracellular signal-regulated kinase kinase 1/2 kinases: mechanism of action *in vivo*, pharmacokinetic/pharmacodynamic relationship, and potential for combination in preclinical models. Mol Cancer Ther 2007;6:2209–19.
14. Flaherty KT. Sorafenib: delivering a targeted drug to the right targets. Expert Rev Anticancer Ther 2007;7:617–26.
15. Rini BI. Sorafenib. Expert Opin Pharmacother 2006;7:453–61.
16. Strumberg D. Preclinical and clinical development of the oral multikinase inhibitor sorafenib in cancer treatment. Drugs Today (Barc) 2005;41:773–84.
17. Gollob JA. Sorafenib: scientific rationales for single-agent and combination therapy in clear-cell renal cell carcinoma. Clin Genitourin Cancer 2005;4:167–74.
18. Rahmani M, Davis EM, Bauer C, Dent P, Grant S. Apoptosis induced by the kinase inhibitor BAY 43-9006 in human leukemia cells involves down-regulation of Mcl-1 through inhibition of translation. J Biol Chem 2005;280:35217–27.
19. Rahmani M, Nguyen TK, Dent P, Grant S. The multikinase inhibitor sorafenib induces apoptosis in highly imatinib mesylate-resistant bcr/abl+ human leukemia cells in association with signal transducer and activator of transcription 5 inhibition and myeloid cell leukemia-1 down-regulation. Mol Pharmacol 2007; 72:788–95.
20. Dasmahapatra G, Yerram N, Dai Y, Dent P, Grant S. Synergistic interactions between vorinostat and sorafenib in chronic myelogenous leukemia cells involve Mcl-1 and p21CIP1 down-regulation. Clin Cancer Res 2007;13:4280–90.
21. Rahmani M, Davis EM, Crabtree TR, et al. The kinase inhibitor sorafenib induces cell death through a process involving induction of endoplasmic reticulum stress. Mol Cell Biol 2007;27:5499–513.
22. Gregory PD, Wagner K, Horz W. Histone acetylation and chromatin remodeling. Exp Cell Res 2001;265:195–202.
23. Marks PA, Miller T, Richon VM. Histone deacetylases. Curr Opin Pharmacol 2003;3:344–51.
24. Bali P, Pranpat M, Swaby R, et al. Activity of suberoylanilide hydroxamic Acid against human breast cancer cells with amplification of her-2. Clin Cancer Res 2005;11:6382–9.
25. Kwon SH, Ahn SH, Kim YK, et al. Apicidin, a histone deacetylase inhibitor, induces apoptosis and Fas/Fas ligand expression in human acute promyelocytic leukemia cells. J Biol Chem 2002;277: 2073–80.
26. Pang RW, Poon RT. From molecular biology to targeted therapies for hepatocellular carcinoma: the future is now. Oncology 2007;72 Suppl 1:30–44.
27. Venturelli S, Armeanu S, Pathil A, et al. Epigenetic combination therapy as a tumor-selective treatment approach for hepatocellular carcinoma. Cancer 2007;109:2132–41.
28. Wise LD, Turner KJ, Kerr JS. Assessment of developmental toxicity of vorinostat, a histone deacetylase inhibitor, in Sprague-Dawley rats and Dutch Belted rabbits. Birth Defects Res Part B Dev Reprod Toxicol 2007;80:57–68.
29. Zhang G, Park MA, Mitchell C, et al. Vorinostat and sorafenib synergistically kill tumor cells via FLIP suppression and CD95 activation. Clin Cancer Res 2008;14:5385–99.
30. Park MA, Zhang G, Martin AP, et al. Vorinostat and sorafenib increase ER stress, autophagy and apoptosis via ceramide-dependent CD95 and PERK activation. Cancer Biol Ther 2008;7: 1648–62.
31. Park MA, Zhang G, Mitchell C, et al. Mitogen-activated protein kinase kinase 1/2 inhibitors and 17-allylamino-17-demethoxygeldanamycin synergize to kill human gastrointestinal tumor cells *in vitro* via suppression of c-FLIP-s levels and activation of CD95. Mol Cancer Ther 2008;7:2633–48.
32. Yacoub A, Park MA, Gupta P, et al. Caspase-, cathepsin- and PERK-dependent regulation of MDA-7/IL-24-induced cell killing in primary human glioma cells. Mol Cancer Ther 2008;7:297–313.
33. Mitchell C, Park MA, Zhang G, et al. 17-Allylamino-17-demethoxygeldanamycin enhances the lethality of deoxycholic acid in primary rodent hepatocytes and established cell lines. Mol Cancer Ther 2007;6:618–32.
34. Gupta S, Natarajan R, Payne SG, et al. Deoxycholic acid activates the c-Jun N-terminal kinase pathway via FAS receptor activation in primary hepatocytes. Role of acidic sphingomyelinase-mediated ceramide generation in FAS receptor activation. J Biol Chem 2001; 279:5821–8.
35. Qiao L, Studer E, Leach K, et al. Deoxycholic acid (DCA) causes ligand-independent activation of epidermal growth factor receptor (EGFR) and FAS receptor in primary hepatocytes: inhibition of EGFR/mitogen-activated protein kinase-signaling module enhances DCA-induced apoptosis. Mol Biol Cell 2001; 12:2629–45.
36. Zhang G, Park MA, Mitchell C, et al. Multiple cyclin kinase inhibitors promote bile acid-induced apoptosis and autophagy in primary hepatocytes via p53 -CD95-dependent signaling. J Biol Chem 2008; 283:24343–58.
37. Mukhopadhyay A, Saddoughi SA, Song P, et al. Direct interaction between the inhibitor 2 and ceramide via sphingolipid-protein binding is involved in the regulation of protein phosphatase 2A activity and signaling. FASEB J 2009;23:751–63.
38. Wegrzyn J, Potla R, Chwae YJ, et al. Function of mitochondrial Stat3 in cellular respiration. Science 2009;323:793–7.
39. Reinehr R, Häussinger D. Hyperosmotic activation of the CD95 system. Methods Enzymol 2007;428:145–60.
40. Pewzner-Jung Y, Ben-Dor S, Futerman AH. When do Lasses

Published OnlineFirst July 14, 2010; DOI: 10.1158/0008-5472.CAN-10-0999

(longevity assurance genes) become CerS (ceramide synthases)?: insights into the regulation of ceramide synthesis. J Biol Chem 2006;281:25001–5.

41. Rosato RR, Almenara JA, Maggio SC, et al. Role of histone deacetylase inhibitor-induced reactive oxygen species and DNA damage in LAQ-824/fludarabine antileukemic interactions. Mol Cancer Ther 2008;7:3285–97.
42. Mikkelsen RB, Wardman P. Biological chemistry of reactive oxygen and nitrogen and radiation-induced signal transduction mechanisms. Oncogene 2003;22:5734–54.
43. Roy SS, Madesh M, Davies E, Antonsson B, Danial N, Hajnóczky G. Bad targets the permeability transition pore independent of Bax or Bak to switch between Ca^{2+}-dependent cell survival and death. Mol Cell 2009;33:377–88.
44. White-Gilbertson S, Mullen T, Senkal C, et al. Ceramide synthase 6 modulates TRAIL sensitivity and nuclear translocation of active caspase-3 in colon cancer cells. Oncogene 2009;28:1132–41.
45. Walker T, Mitchell C, Park MA, et al. Sorafenib and vorinostat kill colon cancer cells by CD95-dependent and -independent mechanisms. Mol Pharmacol 2009;76:342–55.
46. Martin AP, Park MA, Mitchell C, et al. BCL-2 family inhibitors enhance histone deacetylase inhibitor and sorafenib lethality via autophagy and overcome blockade of the extrinsic pathway to facilitate killing. Mol Pharmacol 2009;76:327–41.

AACR American Association for Cancer Research

Cancer Research

The Journal of Cancer Research (1916–1930) | The American Journal of Cancer (1931–1940)

Vorinostat and Sorafenib Increase CD95 Activation in Gastrointestinal Tumor Cells through a Ca^{2+}-*De novo* Ceramide-PP2A-Reactive Oxygen Species–Dependent Signaling Pathway

Margaret A. Park, Clint Mitchell, Guo Zhang, et al.

Cancer Res 2010;70:6313-6324. Published OnlineFirst July 14, 2010.